

Comprehensive control of steering and braking via a 4WIS-4WID vehicle

Yulong Lei*, Guanzheng Wen**, Xiaohu Geng**, Yao Fu***, Xingzhong Li*** and Jianlong Hu****

Keywords: sliding mode control, neural network PID control, comprehensive control strategy, 4WIS-4WID.

ABSTRACT

Four-wheel independent steering and four-wheel independent driving (4WIS-4WID) vehicles have multiple degrees of control freedom. Thus, these vehicles have considerable development potential. However, 4WIS-4WID vehicles easily cause coupling interference between the steering and braking systems. Such interference leads to remarkable difficulties in the design and optimisation of the control system. The comprehensive control of the two systems is realised on the basis of 4WIS-4WID vehicles in this paper. Such control solves the coupling problem between the two systems and achieves improved handling performance whilst guaranteeing the braking stability. This paper mainly includes two parts. Firstly, the linear two degrees-of-freedom model is regarded as a reference model, and a sliding-mode controller is designed to achieve good handling performance. Secondly, a neural network PID cooperative controller is designed to maintain braking stability whilst ensuring handling performance. Lastly, a Simulink/CarSim joint simulation is conducted to confirm the good performance of the proposed strategy.

Paper Received February, 2019. Revised April, 2020. Accepted December, 2020. Author for Correspondence: Guanzheng Wen.

**Professor, State Key Laboratory of Automotive Simulation and Control, Jilin University, Changchun, China.*

***Graduate Student, State Key Laboratory of Automotive Simulation and Control, Jilin University, Changchun, China.*

****Associate Professor, State Key Laboratory of Automotive Simulation and Control, Jilin University, Changchun, China.*

*****Graduate Student, Qingdao Automotive Research Institute, Jilin University, Qingdao, China.*

INTRODUCTION

Four-wheel independent steering and four-wheel independent driving (4WIS-4WID) vehicles are a perfect automatic driving platform with distributed actuators, which can realise independent steering and braking operation. These vehicles have remarkable development potential and have been widely emphasised at home and abroad [Guoying et al, 2019]. Compared with a conventional vehicle, a full drive-by-wire 4WIS-4WID vehicle reduces numerous transmission parts and has high transmission efficiency, a compact structure and additional available space. The realisation of the coordination and matching of the steering and braking systems of this vehicle type to ensure the stability of vehicle handling is the basis of realising all other functions, including automatic driving. This factor restricts the development of such a vehicle. Therefore, the comprehensive control of the steering and braking systems of a 4WIS-4WID vehicle has become a popular research area. The design and optimisation of a comprehensive control system are challenging because it is a redundant system with many degrees of freedom; this system is also equipped with many distributed actuators, such as independent driving, braking and active steering systems [Ren, 2017].

Junjun Zhu, Zhenpo Wang, Lei Zhang, David G. Dorrell divided the controller into three modules. The monitoring module was used to identify the driver intentions, and the upper module used the particle swarm optimisation algorithm to obtain the desired control force in real time continuously. The lower module also utilised the particle swarm optimisation algorithm to control the braking actuator and steering angle to achieve the optimal performance of the vehicle [Zhu et al, 2019]. Peng hang et al. of Tongji University designed a robust controller based on μ estimation to overcome various interference factors and track the desired trajectory. The weighted least square method was also used to distribute the torque to each wheel to achieve a specific operation. Finally, an integrated control strategy was realised [Hang et al, 2019]. Moustapha Doumiati et al. investigated the coordination of

active front steering (AFS) and rear braking in a driver-assist system for vehicle yaw control and achieved the coordinated control of steering and braking mechanisms through linear parameter varying [Doumiati et al, 2013]. The proposed methods focused on the implementation of hierarchical and integrated control methods but ignored that of the direct yaw control (DYC) and AFS functions despite their easy application for 4WIS–4WID vehicles. Consequently, the robustness and real-time performance of control methods are nonideal.

XIANYI XIE et al. designed the electronic stability control and rear active steering cooperative control system to achieve enhanced vehicle handling and stability based on the $\beta - \dot{\beta}$ phase plane method [Xie et al, 2018]. Long Chen et al. proposed a multi-objective coordinated control strategy that improves the extension mileage and ensures the yaw stability of distributed drive electric vehicles [Chen et al, 2018]. Haiyan Zhao et al. divided the controller into body control, tyre force distribution and lower actuator control layers; they also realised integrated control of the longitudinal, lateral and vertical forces of the distributed driving vehicle and achieved good safety, handling stability, ride comfort and track-tracking performance [Zhao et al, 2019]. Based on the active steering system and direct yaw moment control [Poussot-Vassal et al, 2011, Yang et al, 2009], several control allocation algorithms [Schiebahn et al, 2010, Tjonnas et al, 2009], model predictive control strategies [Di Cairano et al, 2010] and robust control strategies [Guvenc et al, 2003, Guvenc et al, 2008] have been applied to the integrated control of steering and braking systems from various perspectives. The proposed methods have been proven to be theoretically feasible through simulation verification. However, response delays and coupling interferences occur between various actuators. The actuators are also interfered by numerous uncertain factors, which often exceed the stability margin of the set robust control. Therefore, the effect of the proposed control methods is often unsatisfactory.

Overall, 4WIS–4WID vehicles not only have multiple degrees of freedom and can easily implement DYC and AFS functions but also have strong nonlinearity and redundancy. These characteristics result in severe internal and external interferences, which make it difficult to achieve stability and overcome the characteristics of response delay. This paper proposes a comprehensive control strategy based on sliding-mode variable structure and neural network PID controller to solve these problems. This strategy can meet the requirements of handling stability. The major contributions of this paper are as follows.

(1) The sliding-mode variable structure control method based on the reference model is used to

achieve good control stability based on the 4WIS–4WID vehicle.

(2) During braking control, the back propagation (BP) neural network PID control method is used in the comprehensive control strategy. This method can ensure the handling stability and achieve improved braking stability.

Lastly, a Simulink/CarSim joint simulation is conducted. The results show that the comprehensive control method in this paper has high stability and real-time performance.

Vehicle model

Prototype vehicle and its parameters

The concept of 4WIS–4WID vehicles has been proposed in the early 1980s [Hiraoka et al, 2009]. Compared with ordinary electric and traditional fuel vehicles, 4WIS–4WID vehicles can achieve zero radius steering, lateral parking and other functions to improve the handling performance. However, these vehicles have a redundant system with multiple degrees of freedom that allows enhanced dynamic performance but also increases the control difficulty [Ren, 2017].

A 4WIS–4WID vehicle model was preliminarily built before this study. The prototype vehicle and its parameters are shown in Fig. 1 and Table 1, respectively.



Fig. 1. Prototype vehicle.

Table 1. Vehicle parameters.

Parameter	Value
Distance between COG and front axle $l_f(m)$	1.064
Distance between COG and rear axle $l_r(m)$	1.072
Cornering stiffness of front axle $k_f \left(\frac{N}{rad} \right)$	10000
Cornering stiffness of rear axle $k_r \left(\frac{N}{rad} \right)$	14000
Yaw moment of inertia of the mass $I_z(kg \cdot m^2)$	1200
Mass of the vehicle $m(kg)$	990
Mass of the tyre $m_1(kg)$	67.566
Wheel radius $r(m)$	0.4528
Moment of inertia of the wheel $J(kg \cdot m^2)$	13.8549
Vehicle width $b(m)$	1.485
Distance between front and rear axles $l(m)$	2.136

Linear vehicle model of two degrees of freedom

This paper takes the linear two degrees-of-freedom steering model as the reference model because the driver is accustomed to the front wheel steering model. This model is selected to demonstrate the steering intention of the driver intuitively. The actual model is simplified into a single-track model as shown in Figure 2 to facilitate problem analysis.

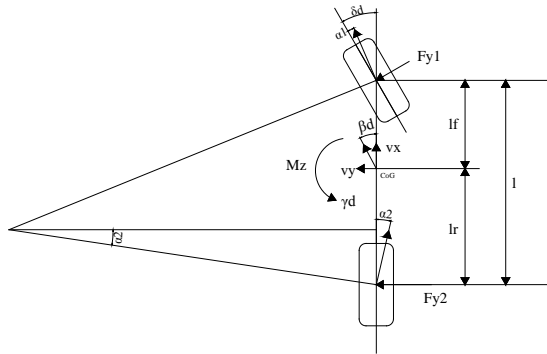


Fig. 2. Single-track model.

Based on the external force of the model, the total lateral force and the total moment around the mass centre are expressed as follows [Doumiati et al, 2013]:

$$\begin{aligned} \sum F_y &= F_{y1} \cdot \cos \delta_d + F_{y2} \\ \sum M_z &= l_f \cdot F_{y1} \cdot \cos \delta_d - l_r \cdot F_{y2}, \end{aligned} \quad (1)$$

Where $\sum F_y$ is the total lateral force; F_{y1} F_{y2} are the lateral forces of the front and rear wheels, respectively, $\sum M_z$ is the total yaw moment and δ_d is the desired steering angle.

From the definition of sideslip angle, the following can be obtained [Ren, 2017]:

$$\begin{aligned} \alpha_1 &= \beta_d + \frac{l_f \cdot \dot{\gamma}_d}{v_x} - \delta_d \\ \alpha_2 &= \beta_d - \frac{l_r \cdot \dot{\gamma}_d}{v_x}, \end{aligned} \quad (2)$$

Where α_1 α_2 are the sideslip angles of the front and rear wheels, respectively; β_d is the desired vehicle sideslip angle, $\dot{\gamma}_d$ is the desired yaw rate and v_x is the longitudinal speed and is a fixed value. The equation can be regarded as a linear relationship between the lateral tyre force and slip angle when the tyre slip angle is assumed to be small. A simplified equation can be obtained as follows:

$$\begin{aligned} F_{y1} &= -k_f \cdot \alpha_f \\ F_{y2} &= -k_r \cdot \alpha_r, \end{aligned} \quad (3)$$

In accordance with the above mentioned relations, the formula of the two degrees-of-freedom model can be obtained as follows[Xie et al, 2018]:

$$\begin{aligned} (k_f + k_r) \cdot \beta_d + \frac{1}{v_x} \cdot (l_f \cdot k_f - l_r \cdot k_r) \cdot \dot{\gamma}_d - k_f \cdot \delta_d &= m \cdot (\dot{v}_y + v_x \cdot \dot{\gamma}_d) \\ (l_f \cdot k_f - l_r \cdot k_r) \cdot \beta_d + \frac{1}{v_x} \cdot (l_f^2 \cdot k_f + l_r^2 \cdot k_r) \cdot \dot{\gamma}_d - l_f \cdot k_f \cdot \delta_d &= I_z \cdot \dot{\gamma}_d, \end{aligned} \quad (4)$$

Four-wheel independent steering model

The four-wheel steering model is simplified as a single-track model as shown in Figure 3 to reduce the design difficulty of the sliding-mode controller.

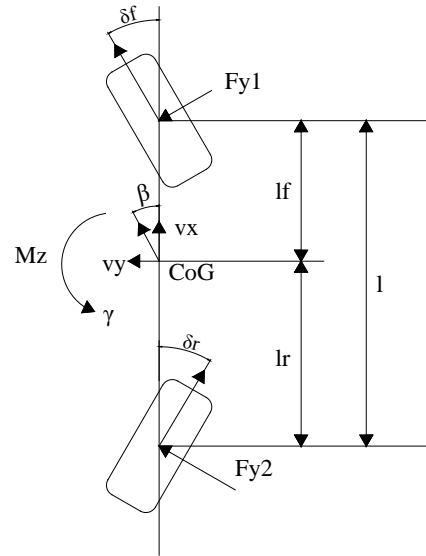


Fig. 3. Four-wheel independent steering single-track model.

The model shows that the 4WIS-4WID vehicle described in this paper has DYC and AFS functions. Accordingly, the dynamic equation can be expressed as follows [Hang et al, 2019]:

$$\begin{aligned} m \cdot (\dot{v}_y + v_x \cdot r) &= F_{y1} \cdot \cos \delta_f + F_{y2} \cdot \cos \delta_r \\ I_z \cdot \dot{\gamma} &= F_{y1} \cdot l_f \cdot \cos \delta_f - F_{y2} \cdot l_r \cdot \cos \delta_r + M_z, \end{aligned} \quad (5)$$

where δ_f is the steering angle of the front wheels, δ_r is the steering angle of the rear wheels and M_z is the additional torque.

The transformation relationship between the model and the actual four-wheel-steering model should meet the Ackermann steering geometry, and its formula is as follows [Hang et al, 2019]:

$$\begin{aligned} \tan \delta_{fl} &= \frac{\tan \delta_f}{1 - \frac{b}{2 \cdot l} \cdot (\tan \delta_f - \tan \delta_r)} \\ \tan \delta_{fr} &= \frac{\tan \delta_f}{1 + \frac{b}{2 \cdot l} \cdot (\tan \delta_f - \tan \delta_r)} \end{aligned}$$

$$\tan \delta_{rl} = \frac{\tan \delta_r}{1 - \frac{b}{2 \cdot l} \cdot (\tan \delta_f - \tan \delta_r)}$$

$$\tan \delta_{rr} = \frac{\tan \delta_r}{1 + \frac{b}{2 \cdot l} \cdot (\tan \delta_f - \tan \delta_r)}, \quad (6)$$

where δ_{fl} δ_{fr} δ_{rl} δ_{rr} are the angles of fl, fr, rl and rr wheels, respectively.

Braking model and anti-lock brake system (ABS)
The single-wheel braking model based on the wheel rotational dynamics is shown in Figure 4.

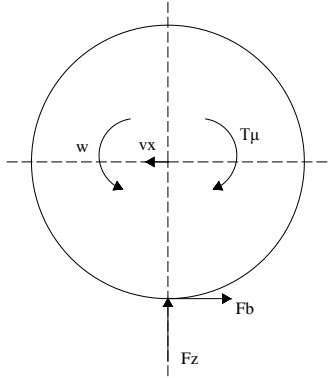


Fig. 4. Single-wheel braking model.

The single-wheel braking model is expressed as follows [Zhu et al, 2019]:

$$F_b = \phi \cdot F_z$$

$$T_\mu = C_p \cdot P$$

$$J \cdot \dot{\omega} = F_b \cdot r - T_\mu, \quad (7)$$

where ϕ is the road adhesion coefficient, w is the wheel speed, T_μ is the braking torque, F_b is the braking force, F_z is the vertical force, C_p is the braking coefficient and P is the brake cylinder pressure.

The relationship amongst the lateral adhesion coefficient, the longitudinal adhesion coefficient and the slip ratio during braking must be identified to determine the value of ϕ . This relationship is shown in the following figure:

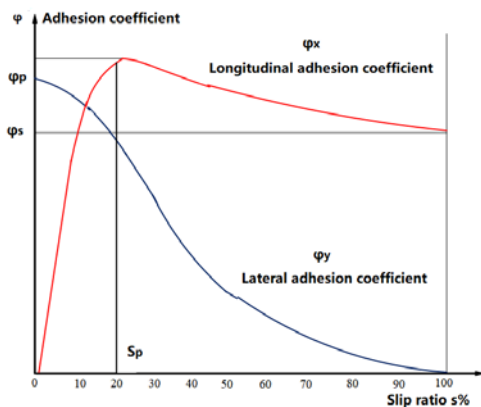


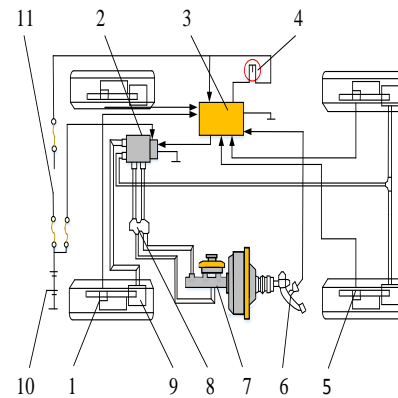
Fig. 5. Relationship between adhesion coefficients and the slip ratio.

The slip ratio is defined as follows [Zhu et al, 2019]:

$$s = \frac{v_{center} - v_{wheel}}{\max(v_{center}, v_{wheel})}, \quad (8)$$

where s is the slip ratio, v_{center} is the centre speed of the wheel and v_{wheel} is the wheel speed.

The function of ABS is to maintain the slip ratio at the position where the longitudinal adhesion coefficient is the largest and the lateral adhesion coefficient is as large as possible to prevent the locking phenomenon during wheel braking and improve the safety. The schematic of the system is as follows [SOHU, 2019].



- 1—Speed sensor of front wheel 2—Adjustment device of brake pressure
- 3—Electronic control unit of ABS 4—Warning lamp of ABS
- 5—Speed sensor of rear wheel 6—Stop light switch
- 7—Master cylinder 8—Proportional distribution valve
- 9—Wheel cylinder 10—Battery 11—The ignition switch

Fig. 6. Schematic of ABS.

The wheel speed and acceleration sensors constantly transmit signals to the ABS controller during the control process. When the locking trend occurs, the ABS controller sends out instructions to decrease the braking torque; when the braking torque drops more than a certain threshold, the ABS controller sends out instructions to increase the braking torque again. Then, the slip ratio is constantly maintained in the ideal position.

Control strategy

The comprehensive control strategy described in this paper aims to coordinate the steering and braking subsystems of the vehicle to avoid the dynamic coupling between the two subsystems. The sliding-mode variable structure control is adopted in the steering system to achieve good handling performance based on the 4WIS-4WID vehicle. By contrast, a neural network PID controller is designed

for the interference of the steering and braking systems to control the braking process, ensure the braking stability and avoid the internal coupling of

the subsystems. The diagram of the controller is shown in Figure 7.

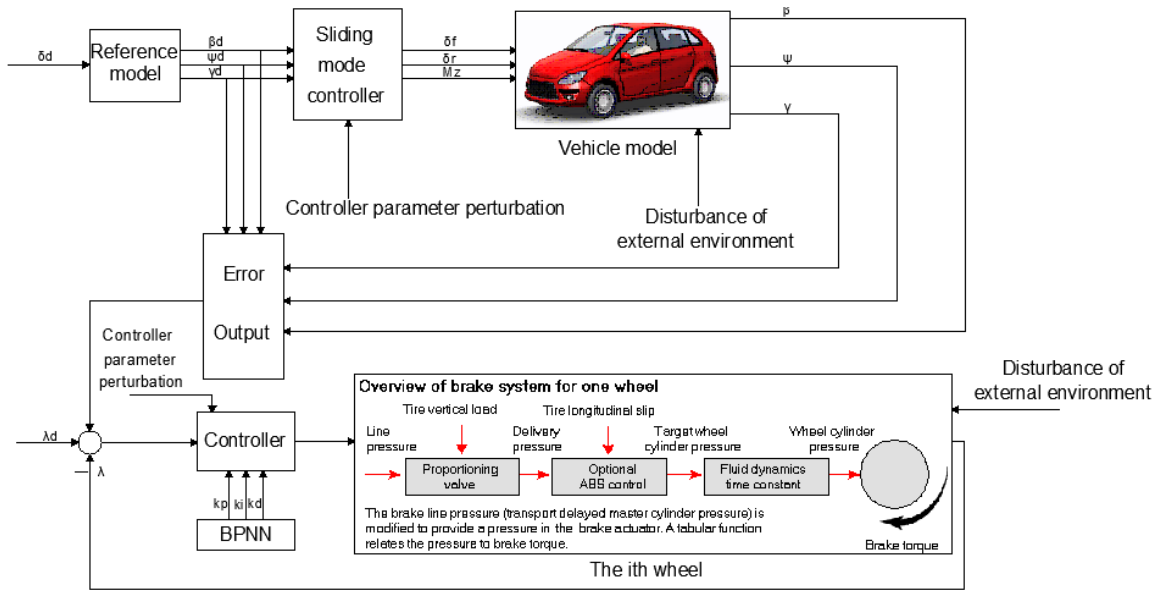


Fig. 7. Diagram of the controller.

The sliding-mode variable structure control method is used during the pure steering process to track β_d , ψ_d , γ_d calculated using the reference model. The strategy can overcome the internal parameter perturbation of the controller and the external disturbance to the vehicle and achieve good tracking performance. In the processes of steering and braking (the nonlinear recombination condition), the actual wheel slip ratio can track the ideal slip ratio by using the BP neural network control. Although these processes have been performed by the sliding-mode control, the error between β_d , ψ_d , γ_d and the corresponding actual value can be eliminated. The BP neural network control can also prevent the internal parameter perturbation of the controller and the external disturbance to the vehicle and eliminate the possible movement interference between the steering and braking subsystems. The control-oriented reference model is shown in formula (10), and the simplified control-oriented vehicle model is shown in formula (11). Eq. (7) shows that the wheel-braking model based on slip ratio control can be obtained as follows [Li et al, 2011]:

$$\dot{s} = \left(1 - s + \frac{m_1 \cdot r^2}{J}\right) \cdot \frac{\dot{v}}{v} + \frac{r}{J \cdot v} \cdot T$$

$$T = C_B \cdot P, \quad (9)$$

where s is the slip ratio, T is the braking torque, C_B is the braking coefficient and P is the brake cylinder pressure, which is also the output of the BP neural network control. Other symbols are shown in Table 1.

Sliding-mode variable structure control

The controller should be stable to maintain the handling performance. Therefore, the sliding-mode variable structure strategy is used to design the controller. This strategy has the advantages of low accuracy of the mathematical model, self-adaptation to internal perturbation and external disturbance, simple control algorithm and easy engineering implementation. Moreover, this strategy can overcome the various interferences and perturbations shown in Figure 7. Based on the proposed reference model, Eq. (3) is converted into a state-space equation [Yu et al, 2006, Li et al, 2011], that is,

$$\dot{X}_d = A_d \cdot X_d + B_d \cdot W_d, \quad (10)$$

Where,

$$X_d = \begin{bmatrix} \beta_d \\ \psi_d \\ \gamma_d \end{bmatrix}, \quad A_d = \begin{bmatrix} 0 & 0 & 0 \\ 0 & 0 & 1 \\ 0 & 0 & -\frac{1}{\tau_d} \end{bmatrix}, \quad B_d = \begin{bmatrix} 0 \\ 0 \\ \frac{k_d}{\tau_d} \end{bmatrix},$$

$$W_d = [\delta_d], \quad \tau_d = \frac{I_z \cdot v_x}{2 \cdot (k_f \cdot l_f^2 + k_r \cdot l_r^2)} \text{ and}$$

$$\tau_d = \frac{I_z \cdot v_x}{2 \cdot (k_f \cdot l_f^2 + k_r \cdot l_r^2)}.$$

Eq. (4), which is a simplified single-track model of the four-wheel steering, is also transformed into a state-space equation, that is,

$$\dot{X} = A \cdot X + B \cdot U, \quad (11)$$

Where,

$$X = \begin{bmatrix} \beta \\ \psi \\ \gamma \end{bmatrix},$$

$$A = \begin{bmatrix} -\left(\frac{k_f+k_r}{m \cdot v_x}\right) & 0 & -\left(\frac{k_f \cdot l_f - k_r \cdot l_r}{m \cdot v_x} + 1\right) \\ 0 & 0 & 1 \\ \frac{k_f \cdot l_f - k_r \cdot l_r}{I_z} & 0 & -\left(\frac{k_f \cdot l_f^2 + k_r \cdot l_r^2}{I_z \cdot v_x}\right) \end{bmatrix},$$

$$B = \begin{bmatrix} \frac{k_f}{m \cdot v_x} & \frac{k_r}{m \cdot v_x} & 0 \\ 0 & 0 & 0 \\ \frac{k_f \cdot l_f}{I_z} & \frac{-k_r \cdot l_r}{I_z} & \frac{1}{I_z} \end{bmatrix},$$

$$U = \begin{bmatrix} \delta_f \\ \delta_r \\ M_d \end{bmatrix}.$$

For the difference in state variables, the following is

The control input is computed as follows to ensure the stability of the control system.

$$U = \begin{bmatrix} U1 \\ U2 \\ U3 \end{bmatrix} = \begin{bmatrix} \frac{d_1}{d_2} \cdot \beta - \eta_1 \cdot \text{sgn}(s) \\ \frac{d_3}{d_4} \cdot \gamma \\ \frac{k_d \cdot I_z}{\tau_d} \cdot \delta_d - \frac{2 \cdot (k_f \cdot l_f \cdot l_f + k_r \cdot l_r \cdot l_r)}{v_x} \cdot \gamma_d - \eta_2 \cdot \text{sgn}(s) \end{bmatrix}, \tag{14}$$

Where $\eta_1 = 0.04$, and $\eta_2 = 0.8$.

The stability of the control system in accordance with the control input is then proven.

From switching function (13), $s = e_1 + e_2$. In accordance with the Lyapunov function, let

$$V = 0.5 \cdot s^2, \tag{15}$$

Then,

$$\dot{V} = s \cdot \dot{s}, \tag{16}$$

$\dot{V} = s \cdot (\dot{e}_1 + \dot{e}_2) = s \cdot (\dot{x}_1 - \dot{x}_{d1} + \dot{x}_3 - \dot{x}_{d3})$ can be determined. If the state-space expression (11) and controller input (14) are integrated, then the following can be obtained:

$$\begin{aligned} \dot{x}_1 &= \dot{\beta} = \frac{k_f+k_r}{m \cdot v_x} \cdot \beta - \left(\frac{k_f \cdot l_f - k_r \cdot l_r}{m \cdot v_x} + 1\right) \cdot \gamma + U_1 \cdot \\ &\frac{k_f}{m \cdot v_x} + \frac{k_r}{m \cdot v_x} \cdot U_2, \\ \dot{x}_{d1} &= 0, \\ \dot{x}_3 &= \dot{\gamma} = \frac{k_f \cdot l_f - k_r \cdot l_r}{I_z} \cdot \beta - \frac{k_f \cdot l_f \cdot l_f + k_r \cdot l_r \cdot l_r}{v_x \cdot I_z} \cdot \gamma \\ &+ \frac{k_f \cdot l_f}{I_z} \cdot U_1 - \frac{k_r \cdot l_r}{I_z} \cdot U_2 + \frac{U_3}{I_z}, \\ \dot{x}_{d3} &= \frac{-\gamma_d}{\tau_d} + \frac{k_d}{\tau_d} \cdot \delta_d, \end{aligned} \tag{17}$$

obtained:

$$E = \begin{bmatrix} e_1 \\ e_2 \\ e_3 \end{bmatrix} = \begin{bmatrix} \beta_d - \beta \\ \psi_d - \psi \\ \gamma_d - \gamma \end{bmatrix}, \tag{12}$$

For the sliding-mode variable structure controller, the switching function is as follows:

$$S = C \cdot E, \tag{13}$$

where C is the coefficient of switching function, $C = [1 \ 0 \ 1]$. Then we can make:

$$\begin{aligned} d_1 &= \frac{k_f+k_r}{m \cdot v_x} - \frac{k_f \cdot l_f - k_r \cdot l_r}{I_z}, \\ d_2 &= \frac{k_f}{m \cdot v_x} + \frac{k_r \cdot l_r}{I_z}, \\ d_3 &= \frac{k_f \cdot l_f - k_r \cdot l_r}{m \cdot v_x \cdot v_x} + \frac{k_f \cdot l_f \cdot l_f + k_r \cdot l_r \cdot l_r}{I_z \cdot v_x} + 1, \\ d_4 &= \frac{k_r}{m \cdot v_x} - \frac{k_r \cdot l_r}{I_z} \end{aligned}$$

Then, $U_1 \ U_2 \ U_3$ and d_1, d_2, d_3, d_4 are brought in, we can get:

$$\dot{V} = s \cdot (-\eta_1 \cdot \text{sgn}(s) - \eta_2 \cdot \text{sgn}(s)) = -\eta_1 \cdot |s| - \eta_2 \cdot |s|, \tag{18}$$

where $V \leq 0$. Therefore, the control input in this study satisfies the stability condition, and the proof is complete.

Eq. (14) concludes that the system can be called forward complete. The specific proof procedure is referred to [David et al, 1999] given the limitation in the length of the article and the specific research areas of this paper.

Comprehensive control of BP Neural Network PID for steering and braking

BP neural network is one of the most mature neural network algorithms because of its simple structure, small computation and good parallelism. PID controller also has the characteristics of simple principle, strong adaptability, reliability and maturity. Therefore, a neural network PID controller is designed in this paper to meet the tracking performance of the steering trajectory and braking stability [Liu et al, 2004]. The error is expressed as follows:

$$e^{BPpid} = s_d - s + M \cdot E, \quad (19)$$

where $M = [0.005 \ 0.005 \ 0.005]$, which is a constant coefficient matrix. In addition to the difference between the ideal and actual slip ratios, e^{BPpid} also has three other errors considering the steering tracking performance. It is close to zero via BP neural network PID adjustment and can meet the performance requirements of steering and braking.

A BP neural network comprises input, hidden and output layers. In this paper, the proportional, integral and differential coefficients of the PID controller are adjusted using this network to adapt to the changes in working conditions constantly and keep e^{BPpid} close to 0. The network diagram is shown in Figure 8.

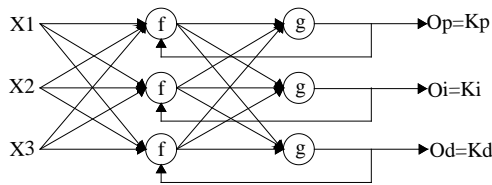


Fig. 8. Diagram of the network.

In the figure, the activation function of the hidden layer is $f(x) = \frac{\exp(x) - \exp(-x)}{\exp(x) + \exp(-x)}$, whilst that of the output layer is $g(x) = \frac{\exp(x)}{\exp(x) + \exp(-x)}$. The weight coefficient between the hidden and input layers is $w_{11}, w_{12}, w_{13}, w_{21}, w_{22}, w_{23}, w_{31}, w_{32}, w_{33}$. The weight coefficient between the output and hidden layers is $j_{11}, j_{12}, j_{13}, j_{21}, j_{22}, j_{23}, j_{31}, j_{32}, j_{33}$.

According to [Liu et al, 2004], during the signal forward propagation, the input to the hidden layer node is computed as follows:

$$m_i = \sum_{j=1}^3 w_{ij} \cdot x_j \quad (i = 1,2,3), \quad (20)$$

The output of the hidden layer node is:

$$mo_i = f(m_i) = f(\sum_{j=1}^3 w_{ij} \cdot x_j) \quad (i = 1,2,3), \quad (21)$$

The input of the output layer node is:

$$net_i = \sum_{j=1}^3 j_{ij} \cdot mo_j \quad (i = 1,2,3), \quad (22)$$

The output of the output layer node is:

$$out_i = g(net_i) = g(\sum_{j=1}^3 j_{ij} \cdot mo_j) \quad (i = 1,2,3), \quad (23)$$

During the BP of the error, for each sample $k = 1,2,3 \dots K$, K is the total number of samples. Let its error function be:

$$J_k = \frac{1}{2} \cdot \sum_{n=1}^N (e_k^{BPpid})^2, \quad (24)$$

where N is the total number of training. Then, the total error function is as follows:

$$J = \frac{1}{2} \cdot \sum_{k=1}^K \sum_{n=1}^N (e_k^{BPpid})^2, \quad (25)$$

The weight coefficient of the output layer is corrected as follows:

$$\Delta j_{ij} = \vartheta_1 \cdot \frac{\partial J}{\partial j_{ij}} = \vartheta_1 \cdot \frac{\partial J}{\partial out_i} \cdot \frac{\partial out_i}{\partial net_i} \cdot \frac{\partial net_i}{\partial j_{ij}}, \quad (26)$$

Where ϑ_1 is the adjustment coefficient.

The weight coefficient of the hidden layer is corrected as

$$\Delta w_{ij} = \vartheta_2 \cdot \frac{\partial J}{\partial w_{ij}} = \vartheta_2 \cdot \frac{\partial J}{\partial mo_i} \cdot \frac{\partial mo_i}{\partial m_i} \cdot \frac{\partial m_i}{\partial w_{ij}}, \quad (27)$$

Where ϑ_2 is the adjustment coefficient.

During the training cycle, each new weight coefficient generated is

$$w_{ij}(k+1) = w_{ij}(k) + \pi_1 \cdot \Delta w_{ij}(k)$$

$$j_{ij}(k+1) = j_{ij}(k) + \pi_2 \cdot \Delta j_{ij}(k) \quad (28)$$

Where π_1, π_2 are the adjustment coefficients. The flow chart of the entire BP neural network PID controller is presented below.

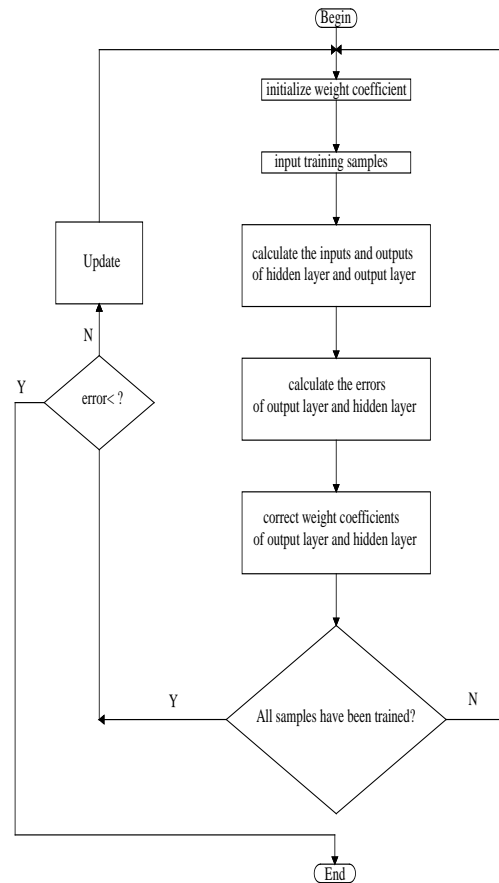


Fig. 9. Flow chart of the BP neural network PID controller.

The BP neural network PID controller regulates the three parameters k_p, k_i, k_d of the PID controller by using the neural network, which is still a PID control. The stability proof method of PID control is relatively mature. The stability proof of the BP

neural network PID control is indicated in [Zhang et al, 2011].

For the two control methods involved in this study, the stability proof of the sliding-mode control was previously described, and the stability of the BP neural network PID control can be referred to [Zhang et al, 2011]. Thus, the stability of the entire closed-loop system can be guaranteed.

After continuous training of the proposed algorithm, the output of the controller can be constantly corrected, and the braking torque of the four wheels can be controlled precisely. Thus, the vehicle always has good braking stability.

Simulation

This paper designs the control strategy based on Simulink and builds the 4WIS-4WID vehicle model using CarSim commercial software to achieve the Simulink/CarSim joint simulation to verify the performance of the proposed comprehensive control method. The handling performance, which is of sliding control, is firstly verified in the simulation. The random curve and step curve are inputted to test the controller performance, as shown in Figure 10.

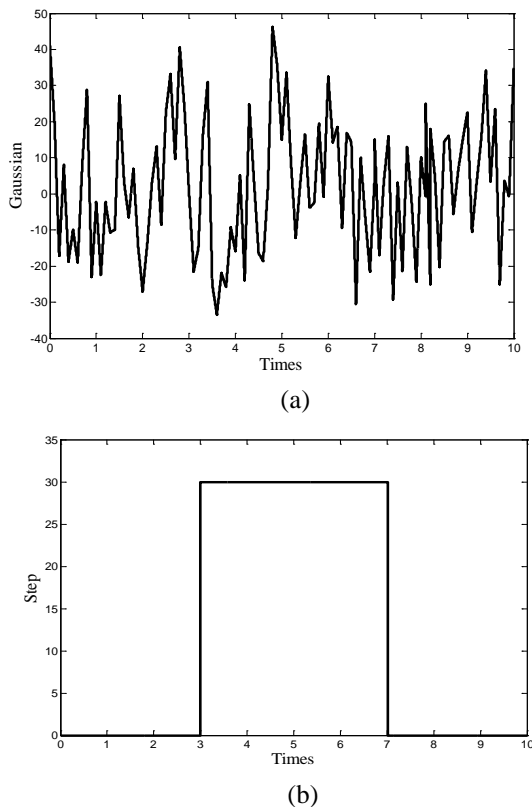


Fig. 10. Input signal.

These inputs do not exist in the actual driving situation. However, the inputs can simulate the extreme driving conditions and test the transient response and tracking performance of the vehicle

control strategy. The proposed control strategy is compared with the traditional PID control method to verify its performance.

Under the condition of the random input of steering wheel angle, the tracking performance is shown as follows:

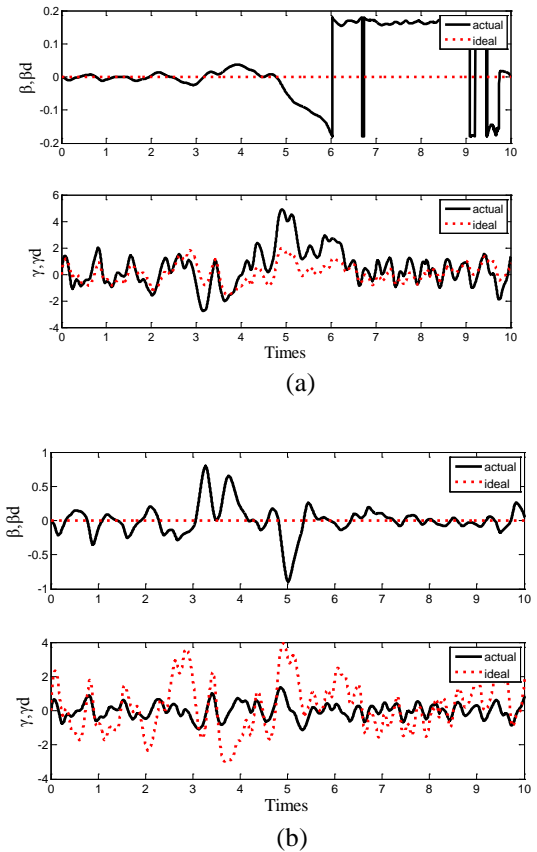


Fig. 11. Ideal and actual responses of random input.

Fig. 11(a) shows the control performance of the proposed controller, whilst Fig. 11(b) shows that of the PID controller. The difference amongst the actual sideslip angle, the yaw rate of the vehicle and the ideal value in Fig. 11(a) is smaller than that in Fig.11(b). Fig. 11(a) indicates that the error of the sideslip angle of the mass centre is less than 0.2, and the error of the yaw rate is very small during most time. Both errors are better than those in Fig. 11(b).

Under the condition of the step input of steering wheel angle, if a 30° angle is inputted at 3 s, then its tracking performance is as follows:

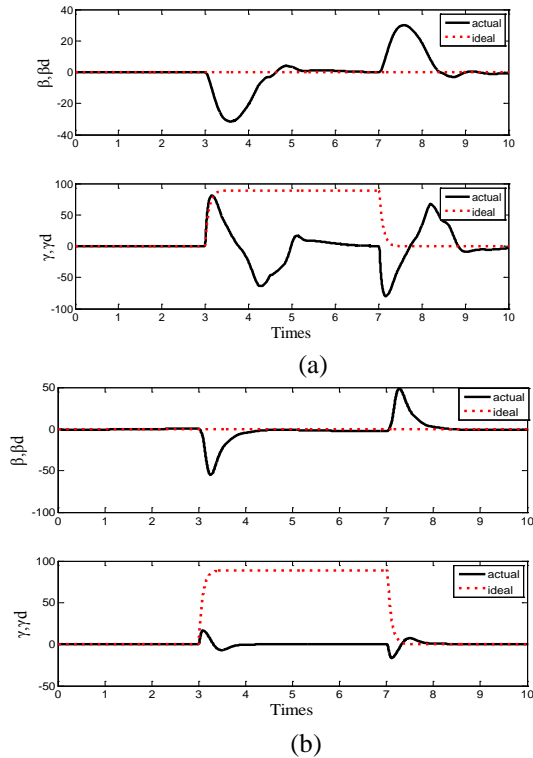


Fig. 12. Ideal and actual responses of step input.

Fig. 12(a) shows the control performance of the proposed controller, whilst Fig. 12(b) shows that of the PID controller. Fig. 12 demonstrates that the proposed controller has less shock than that of the PID controller. At the moment of the input of step signal, the lateral side slip angle of the mass centre and the yaw rate show remarkable oscillations compared with those of the ideal value. Although the PID method converges to 0 earlier, it has a larger shock than that of the proposed controller.

After verifying the handling performance, the braking stability during the nonlinear recombination condition is confirmed by using the BP neural network PID method. The ideal slip ratio is 0.2 under the normal condition. In the nonlinear recombination condition, along with the control of the BP neural network PID method, the tracking performance is as follows:

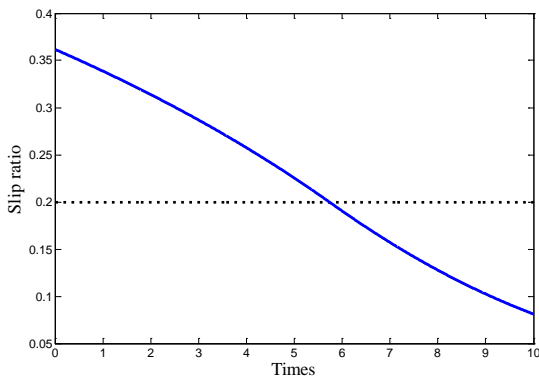


Fig. 13. Tracking performance of the proposed

method.

The actual slip ratio can be always kept around 0.2 using the comprehensive control strategy, that can maintain the braking stability to the largest extent. Compared with the slip ratio of traditional vehicles without special control methods under the same condition, the slip ratio is presented below.

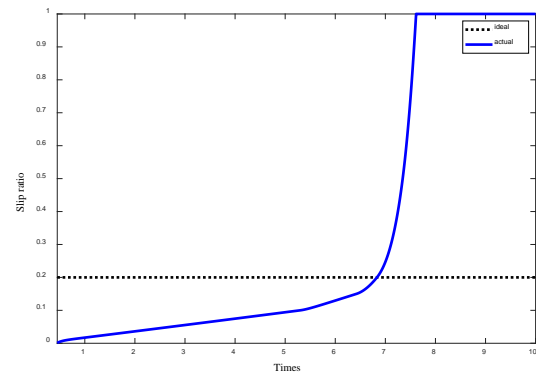


Fig. 14. Tracking performance without special control methods.

After the simulation reaches 7 s, the actual slip ratio is equal to 1, indicating the braking stability loss in the vehicle.

Overall, the comprehensive control strategy has a good stability and real-time performance. Moreover, this strategy can ensure the handling stability of the 4WIS-4WID vehicle and achieve high braking efficiency and stability.

Summary and conclusions

A comprehensive control strategy based on sliding-mode variable structure and BP neural network PID controller is established in this paper to achieve the comprehensive control of the steering and braking systems of a 4WIS-4WID vehicle. The comprehensive control method overcomes the strong nonlinearity between steering and braking actuators, thereby achieving good handling and braking performance. The sliding-mode variable structure control method overcomes the interference of the braking system and the steering system, indicating good handling performance. The BP neural network PID control method achieves the tracking of ideal slip ratio and has a good braking performance. Lastly, the proposed comprehensive control method is verified to have a good stability and real-time tracking performance through a Simulink/CarSim joint simulation. A 4WIS-4WID vehicle is also constructed to verify the reliability of

the proposed comprehensive control method. After the preparation of the experimental site, a real vehicle test will be conducted in the future.

Acknowledgements

The authors would like to thank the National Key Research and Development Program of China, the Science and Technology Planning Project of Jilin Province, the Science and Technology Planning Project of Jilin Province, and Science and Technology Project of Qingdao for providing the authors with their support.

Disclosure statement

No potential conflict of interest was reported by the authors.

Funding

This work was supported by the National Key Research and Development Program of China [grant number 2018YFB0104901]; the Science and Technology Planning Project of Jilin Province [grant number 20160519008JH]; the Science and Technology Planning Project of Jilin Province [grant number 20170204073GX]; the Science and Technology Project of Jilin Provincial Department of Education (No. JJKH20200963KJ); and Science and Technology Project of Qingdao [grant number 18-1-2-17-zhc].

References

- Chen, L., Chen, T., Xu, X., et al., "Multi-objective coordination control strategy of distributed drive electric vehicle by orientated tire force distribution method,"; IEEE Access. Vol. 6, pp. 69559-69574(2018).
- Doumiati, M., Sename, O., Dugard, L., et al., "Integrated vehicle dynamics control via coordination of active front steering and rear braking,"; European Journal of Control, Vol. 19, No. 2, pp. 121-143(2013).
- Di Cairano, S., Tseng, H. E., "Driver-assist steering by active front steering and differential braking: design, implementation and experimental evaluation of a switched model predictive control approach,"; 49th IEEE Conference on Decision and Control (CDC). IEEE, pp. 2886-2891(2010).
- David Angeli, Eduardo D. Sontag. "Forward completeness, unboundedness observability, and their Lyapunov characterizations"; [J]. Systems & Control Letters (1999).
- Guoying, et al., "Comprehensive chassis control strategy of FWIC-EV based on sliding mode control,"; Intelligent Transport Systems, IET (2019).
- Guvenc, B.A., Acarman, T., Guvenc, L., "Coordination of steering and individual wheel braking actuated vehicle yaw stability control,"; IEEE IV2003 Intelligent Vehicles Symposium. Proceedings (Cat. No. 03TH8683). IEEE, pp. 288-293(2003).
- Guvenc, B. A., Guvenc, L., Karaman, S., "Robust yaw stability controller design and hardware-in-the-loop testing for a road vehicle,"; IEEE Transactions on Vehicular Technology, Vol. 58, No. 2, pp. 555-571(2008).
- Hang, P., Chen, X., "Integrated chassis control algorithm design for path tracking based on four-wheel steering and direct yaw-moment control,"; Proceedings of the Institution of Mechanical Engineers, Part I: Journal of Systems and Control Engineering. Vol.233, No.6, pp. 625-641(2019).
- Hiraoka, Toshihiro, O. Nishihara, and H. Kumamoto, "Automatic path-tracking controller of a four-wheel steering vehicle,"; Vehicle System Dynamics Vol.47, No. 10, pp. 1205-1227(2009).
- Li Guo, Feng Zebin, "Cooperative Error Control of Automotive Steering/Anti-lock Braking System,"; Ordnance journal, Vol. 32, No. 9, pp. 1071-1076 (2011).
- Liu Jinkun, "Matlab simulation of advanced PID control (2nd Edition) · ", Publishing House of Electronics Industry, pp.153-165(2004).
- Poussot-Vassal, C., Sename, O., Dugard, L., et al., "Vehicle dynamic stability improvements through gain-scheduled steering and braking control,"; Vehicle System Dynamics, Vol.49, No. 10, pp. 1597-1621 (2011).
- Ren Bingtao., "Research on Torque Coordinated Optimal Control of Four-wheel Drive Electric Vehicles,"; Ph.D. Thesis, Jilin University (2017).
- Schiebahn, M., Zegelaar, P. W. A., Lakehal-Ayat, M., et al., "The yaw torque influence of active systems and smart actuators for coordinated vehicle dynamics controls,"; Vehicle system dynamics, Vol. 48, No. 11, pp. 1269-1284(2010).
- SOHU AUTO, "Lifan automobile core technology: ignoring safety = destroying happiness", <http://auto.sohu.com/20080125/n254880062.shtml> (2008, accessed 7 December 2019).
- Tjonnas, J., Johansen, T. A., "Stabilization of automotive vehicles using active steering and adaptive brake control allocation,"; IEEE Transactions on Control Systems Technology, Vol. 18, No. 3, pp. 545-558(2009).
- Xie, X., Jin, L., Jiang, Y., et al., "Integrated dynamics control system with ESC and RAS for a distributed electric vehicle,"; IEEE Access, Vol. 6, pp. 18694-18704(2018).
- Yang, X., Wang, Z., Peng, W., "Coordinated control of AFS and DYC for vehicle handling and

stability based on optimal guaranteed cost theory,”; Vehicle System Dynamics, Vol. 47, No. 1, pp. 57-79(2009).

Yu Zhuoping, Gao Xiaojie, Zhang Lijun, “Study on joint control of direct yaw moment and variable wheel slip ratio for vehicle stability control,”; Automobile Engineering, No. 9, pp. 844-848(2006).

Zhu, J., Wang, Z., Zhang, L., et al. “Braking/steering coordination control for in-wheel motor drive electric vehicles based on nonlinear model predictive control,”; Mechanism and Machine Theory. Vol.142(2019).

Zhao, H., Chen, W., Zhao, J., et al., “Modular Integrated Longitudinal, Lateral, and Vertical Vehicle Stability Control for Distributed Electric Vehicles,”; IEEE Transactions on Vehicular Technology, Vol.68, No. 2, pp. 1327-1338(2019).

Zhang Guozheng, Hu Zheng. “Improved BP neural network model and its stability analysis”; [J]. Journal of Central South University (NATURAL SCIENCE EDITION) (2011).

基於四輪獨立轉向獨立驅動車輛的轉向制動綜合控制

雷雨龍 溫官正 耿小虎 付堯
李興忠 扈建龍

吉林大學汽車仿真與控制國家重點實驗室
吉林大學青島汽車研究院

摘要

四輪獨立轉向和獨立驅動車輛具有多個控制自由度，具有很大的發展潛力。但是，這種車輛容易在子系統之間產生耦合幹擾。這些幹擾在車輛控制過程中造成了極大的困難，所以本文設計了綜合控制方法。本文所述控制方法解決了轉向和制動系統之間的耦合問題，並可同時保證制動性能和操縱穩定性。本文主要包括兩個部分：首先，將線性二自由度模型作為參考模型，設計滑模控制器以實現良好的操縱穩定性。其次，設計了神經網PID控制器來同時確保制動性能和操縱穩定性。最後，基於 Simulink / CarSim 軟件進行聯合仿真，驗證了所述控制方法的良好性能。

